Proceedings of the 23rd National Heat and Mass Transfer Conference and 1st International ISHMT-ASTFE Heat and Mass Transfer Conference IHMTC2015
17-20 December, 2015, Thiruvananthapuram, India

Paper No. IHMTC2015- 487

AERO-THERMODYNAMICS OPTIMIZATION OF RE-ENTRY CAPSULE IN THE SLIP FLOW REGIME

Harshal Gijare
MAE Department IIT Hyderabad
Email: me13m15p000002@iith.ac.in

Ashwani Assam
MAE Department IIT Hyderabad
Email: me12m14p000004@iith.ac.in

Nishanth Dongari
MAE Department IIT Hyderabad
Email: nishanth@iith.ac.in

ABSTRACT

We carry out numerical simulations to optimize the re-entry capsule configurations based on aero-thermodynamic properties such as drag, pressure and heat load. The open source software OpenFOAM is used with the compressible computational fluid dynamics (CFD) solver rhoCentralFoam. CFD solver is implemented with the first-order Maxwell's velocity slip and the Smoluchowski temperature jump boundary conditions. We report results for different altitudes and Mach numbers with varying second cone angle and bluntness of the re-entry capsule. It is noted that the heat loads are greatly reduced by changing the capsule configuration from single to bi-cone. With increasing second cone angle heat loads are enhanced, but the average drag and pressure coefficients found to be least sensitive. However, with increase in bluntness the average value of heat load decrease slightly and the peak value significantly, while drag values exhibit contrasting behaviour.

***Keywords*:** Aero-thermodynamics, Re-entry, Slip flow regime, Bi-cone, Bluntness, Trajectory

NOMENCLATURE

Kn Knudsen Number
α, β Angle
D_1, D_2 Capsule Diameters
C_d Drag coefficient
C_h Heat transfer coefficient
U Velocity (m/s)
T Temperature (K)
Ma Mach number
Re Reynolds number
F_d Drag force per unit area
λ Mean free path
q Heat flux
ρ Density (kg/m^3)
∞ Free-stream conditions

INTRODUCTION

A good atmospheric re-entry is when the space vehicle can withstand the extreme aerodynamic heating and make precise landing within the desired range [1]. Therefore, an accurate predictions of aero-thermodynamic loads on a re-entry capsule is imperative for aerospace applications. Thermal protection systems (TPSs) materials research largely depends on these findings [2]. For the efficient operation of hypersonic transport systems such as SpaceLiner [3], the design has to be done with optimum aerodynamic performance [4]. Reentry vehicles are blunted to reduce the heat

load as it is inversely proportional to drag [5]. Lin et al. [6] described optimum bi-cone shape for improving the aero-thermodynamic performance. Wei et al. [7] demonstrated aero-thermodynamic optimization of bi-cone capsule with respect to the lift to drag ratio. Clauser [8] carried out a study of space flight, which further explored the possibility of safe landing, but it did not take into consideration of the high-altitude atmospheric conditions. The focus of current aerospace engineers is now shifting to mimic exo-atmospheric conditions using the limited experimental data and available computational power [9].

The use of extended Navier-Stokes equations by applying the non-equilibrium slip boundary conditions has become popular for improving the accuracy of conventional CFD in the slip and transition flow regimes. In the slip and transition flow regimes (altitude between 40 to 150 km) there is a significant scarcity for experimental data [10], especially heat transfer and temperature. Therefore, the analysis of re-entry aero-thermodynamics in these flow regimes still present a challenging problem. The Navier-Stokes equations along with the no-slip/no-jump boundary conditions yield significantly inaccurate results in the slip and transitional regimes, and require special modifications for taking into account non-equilibrium effects [11, 12]. For a better aero-thermodynamic design of re-entry vehicles we require data that could predict the heat and drag loads at altitude between 50 to 80 km. The vehicle need to make through the above re-entry corridor (the narrow region in space that a re-entering vehicle must fly through, so that the vehicle can make a successful landing without skipping or burning out). Therefore a need to study the aerodynamic heating and drag values for various flow and geometrical configurations is required.

NUMERICAL SIMULATIONS

OpenFoam uses C++ as its base language as it provides the advantage of object-oriented programming language. It incorporates many class libraries for efficient development of CFD codes. Implementation of tensor fields, partial differential equations, boundary conditions and so on, can be handled using these libraries [13]. It has become a popular tool in the scientific and OpenSource CFD community [14, 15].

The *rhoCentralFoam* is the density-based compressible flow solver based on central-upwind schemes of Kurganov and Tadmor [16, 17]. Christopher *et al* [18] has validated this solver against various standard compressible test cases. Bansal *et al.* [19] used this solver along with *reactingFoam* (another solver within OpenFoam) for developing hypersonic flow solver. Various compressible solvers have also been compared wth *rhoCentralFoam* in literature and it is

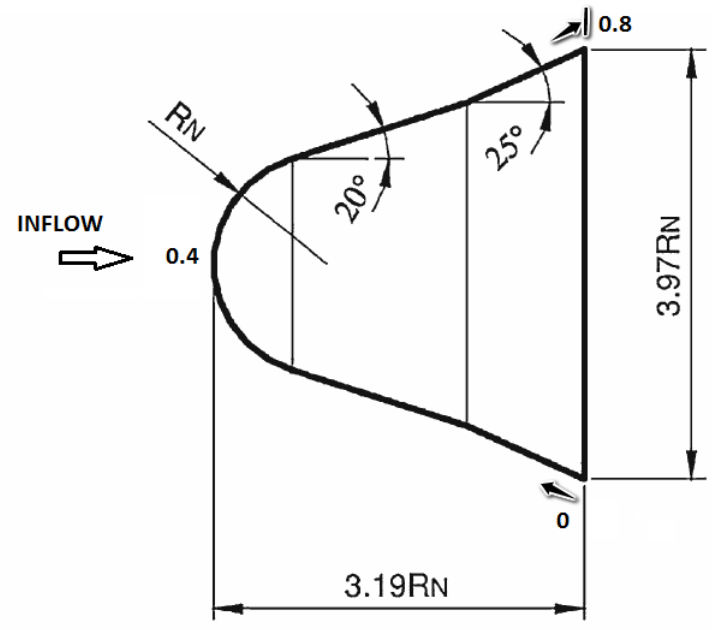

FIGURE 1. BALLISTIC RE-ENTRY CAPSULE (*CROSS-SECTIONAL VIEW*) (THE ARROW SHOWS THE ARC-LENGTH TAKEN ALONG THE CAPSULE WALL.)

shown to predict good results for high speed continuum flows [20]. We have used the 1-equation Spalart Allarmas turbulence model [21]. This model has been validated using OpenFOAM solver for atmospheric-entry capsules at subsonic speed [22]. The accuracy of the Navier-Stokes solver is improved by using the slip boundary conditions for rarefied regime of the flow. The use of Maxwell, Smoluchowski, Langmuir-Maxwell and Langmuir-Smoluchowski (so-called hybrid boundary condition) [23–25] have been incorporated in this solver [26]. Air reaction chemistry and radiation effects are not considered in the current work.

VALIDATION

The *rhoCentralFoam* is validated against wind tunnel experimental data [27] for both the pressure coefficient (C_p) and density (ρ) variation on the capsule wall surface. The capsule configuration chosen is shown in the Fig. 1. The nose radius R_n is taken as 0.1 m for the current investigation. The test conditions are with free-stream pressure 833 Pa, static-temperature of 63 K, Mach number of 5.0 and angle of attack of 4.66. These conditions corresponds to altitude of 33 km which falls in the continuum flow regime.

Comparison of wind-tunnel test data and results for CFD method with the slip and jump boundary conditions (Extended CFD) for pressure coefficient over the surface of

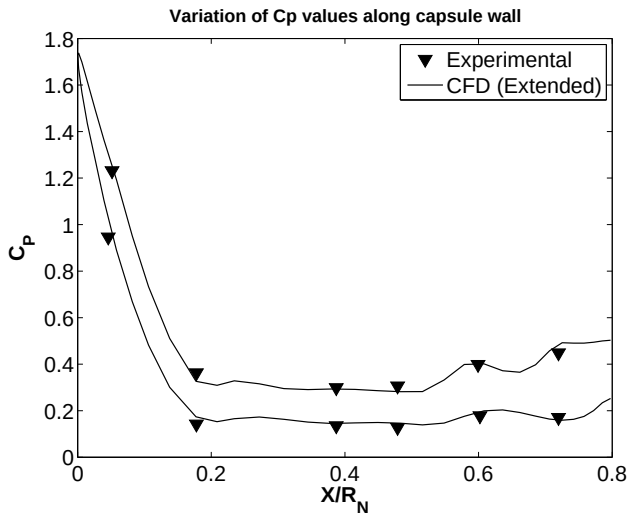

(a)

FIGURE 2. COMPARISON BETWEEN THE WIND-TUNNEL EXPERIMENTAL DATA AND CFD METHODS FOR COEFFICIENT OF PRESSURE (C_P)

re-entry capsule is shown in Fig. 2. As expected, higher pressure is observed at the windward than the leeward side of vehicle. The results from the solver have good agreement with the experimental data. Maximum pressure is observed at the stagnation point or nose of the capsule and pressure remains constant along the surface of capsule till the second cone. A jump in the pressure is observed at the second cone due to the formation of weak shock wave formation. Pressure coefficient is closely matched with the wind-tunnel data near nose of the capsule.

TEST CASES

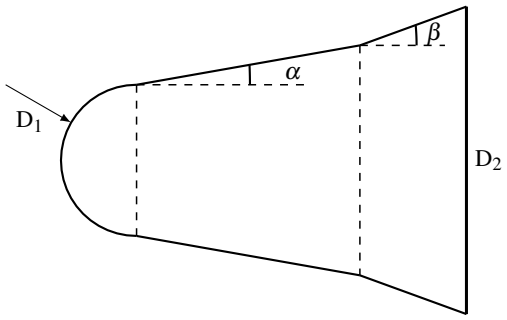

FIGURE 3. CAPSULE SCHEMATIC

We have chosen a re-entry capsule in our current study, a schematic of which is shown in Fig. 3. Maxwell slip and Smoluchowski jump boundary condition is applied on entire capsule wall. The mesh used is structured with multiblock grid with linear grading near wall with smallest mesh size near wall $\delta x = 2.4mm$. Here, α and β denotes the first and second cone angles respectively, D_1 and D_2 are nose cone and base diameters respectively, and L is the length of capsule. The bluntness of the capsule is defined as the ratio of D_1 to D_2. Optimization is carried out based on the average drag coefficient, and average and peak heat load. The parametric study includes β variation from 20° to 40° by keeping the bluntness constant as 0.5. The case of $\alpha = 20^\circ = \beta$ forms a single cone case. The bluntness is then varied from 0.25 to 0.5, by keeping the cone angles constant to decide optimum configuration. The simulations have been performed for altitude 60 km and 70 km (Kn = 0.012 and 0.037, respectively). The various geometrical configurations of the capsule shown in Fig. 3, for which the cases has been considered in this paper are tabulated in table 1.

Cases:	α	β	D_1 **(in m)**	D_2 **(in m)**	Re
Single-Cone	20°	20°	0.2	0.397	6150
Bi-cone:					
(I)	20°	25°	0.2	0.397	6150
(II)	20°	30°	0.2	0.407	6300
(III)	20°	40°	0.2	0.459	7105
Bluntness:					
0.25	20°	25°	0.1	0.397	6150
0.375	20°	25°	0.15	0.397	6150
0.5	20°	25°	0.2	0.397	6150

TABLE 1. VARIOUS GEOMETRIC TEST CASE CONFIGURATIONS

RESULTS AND DISCUSSION

We investigate heat transfer and drag coefficients for aero-thermodyanamic design optimization. Our objective in this study is to come with a configuration with minimum heat flux and drag coefficient.

Drag Coefficient

The drag coefficient C_d along a surface is a measure of net kinetic energy flux of the molecule impinging on the

surface, which is numerically stated as follows

$$C_d = \frac{F_d}{\frac{1}{2}\rho_\infty U_\infty^2} \tag{1}$$

where F_d is the drag force per unit area. It includes both pressure and skin-friction drag.

Coefficient of Heat Transfer

Coefficient of heat transfer C_h along a surface is a measure of net energy flux of the molecule impinging on the surface. It is numerically stated as,

$$C_h = \frac{q_w}{\frac{1}{2}\rho_\infty U_\infty^3}, \tag{2}$$

where q_w is the heat flux ρ_∞ and U_∞ are the freestream density and velocity receptively.

Comparison of Single-cone and Bi-cone Configuration

Figure. 4 shows the comparison of C_d at 70km altitude and Ma = 10. Peak value of the C_d for both configurations is identical. However after formation of second shock wave, the value of C_d is higher for bi-cone configuration due to increase of density. Table 2, shows % deviation of average value of C_d over the entire capsule wall. The flow conditions are Ma = 10, 15 and 20, and at 60 km & 70 km altitude conditions. We have considered higher and different values for Mach numbers as the non-equilibrium effects in momentum transfer is simply governed by Knudsen number whereas non-equilibrium nature of energy transfer is governed by Knudsen as well as Mach number. Thus, a varying Mach number conditions provides a better account for thermal effects. The table shows that the maximum deviation is well below 5%, and it reduces as the altitude increases. In real case scenario, drag coefficient value effects the accuracy in landing such that a lower value of drag coefficient helps in getting a more accurate landing.

Figure 5 demonstrates comparison of heat transfer coefficient at 70km altitude and Ma = 10. This plot shows that peak value of heat transfer coefficient is reduced significantly for bi-cone configuration (35%-40%). We can notice from Fig. 8 that the temperature peak has shifted from the nose towards the downstream location for the bi-cone configuration. This is due to the formation of multiple shocks and their interaction for bi-cone case, see Fig. 6 and 7. This phenomenon is well known as the multiple shock system. Table 3 shows the deviation of average value of heat transfer

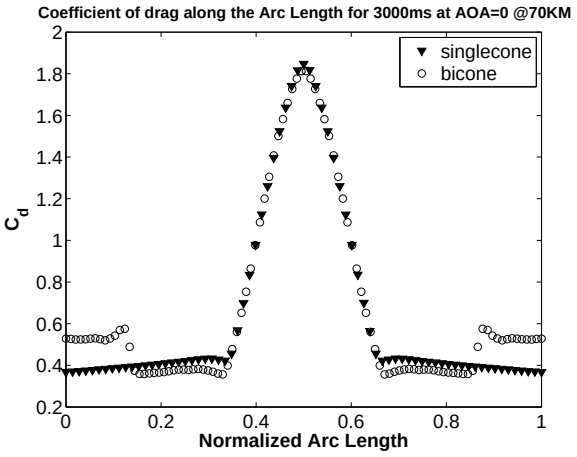

(a)

FIGURE 4. COMPARISON OF DRAG COEFFICIENT ALONG CAPSULE WALL AT 70KM.

coefficient over the entire capsule wall for bi-cone configuration w.r.t single-cone. The value of deviation is around $15\% - 35\%$. So we understand that heat flux acting on the capsule is significantly reduced when the configuration is changed from single to bi-cone. C_h value plays a key role in determining the insulation/ablation layers on the capsule, i.e. the weight of the overall system is reduced and a safer landing can be achieved. Hence, by observing both drag and heat transfer coefficients, we can infer that a bi-cone configuration is aero-thermodyanamically better optimized compared to the single cone case.

Average C_d	60km			70km		
Ma	**10**	**15**	**20**	**10**	**15**	**20**
Single-cone	0.657	0.640	0.635	0.669	0.647	0.639
Bi-cone	0.679	0.663	0.657	0.685	0.666	0.658
%Deviation	3.36	3.54	3.47	2.48	2.85	3.03

TABLE 2. AVERAGE DRAG COEFFICIENT C_D DATA AT 60 KM AND 70 KM ALTITUDE FOR VARIOUS FLOW CONDITIONS.HERE, ABSOLUTE VALUES ARE PRESENTED FOR SINGLE-CONE AND BI-CONE CONFIGURATIONS. DEVIATION DENOTES THE % OF DEVIATION OF BI-CONE WITH SINGLE-CONE CONFIGURATION RESULTS.

Optimizing 'β' Second-cone Angle

Figure 9 and 10 demonstrates the variation of drag and heat transfer coefficient along the entire capsule wall, and

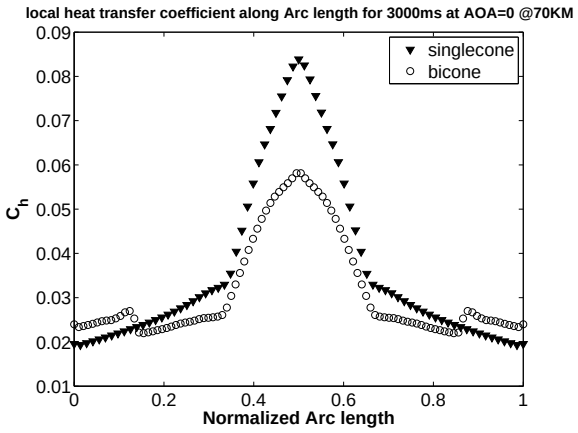

(a)

FIGURE 5. COMPARISON OF LOCAL HEAT TRANSFER COEFFICIENT ALONG CAPSULE WALL AT 70KM.

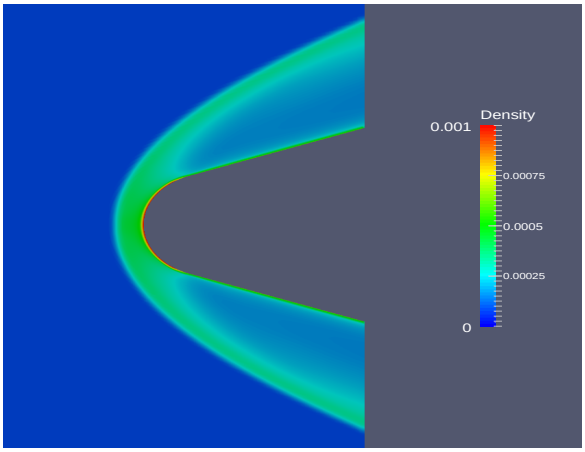

(a)

FIGURE 6. CONTOUR PLOT OF DENSITY FOR SINGLE-CONE CONFIGURATION AT 70KM AND MACH = 10.

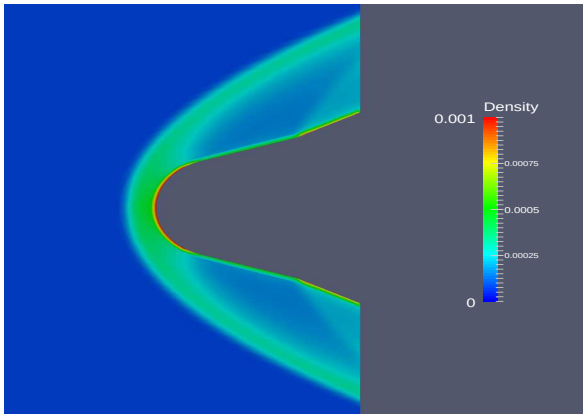

(a)

FIGURE 7. CONTOUR PLOT OF DENSITY FOR BI-CONE CONFIGURATION AT 70KM AND MACH = 10.

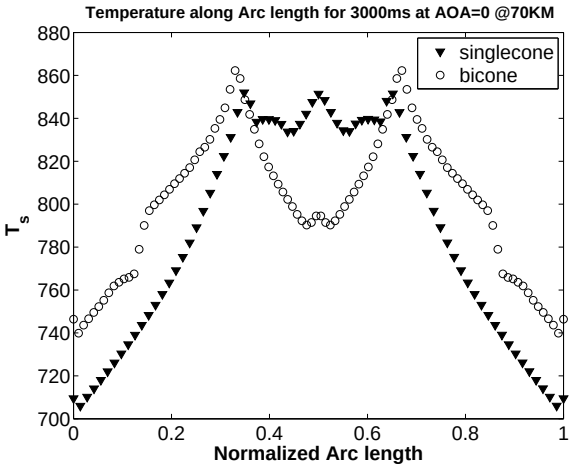

(a)

FIGURE 8. COMPARISON OF TEMPERATURE CAPSULE WALL AT 70KM.

comparison has been made for different values of β. It can be noticed that for $\beta = 25^\circ$ the values of both local heat transfer and drag coefficient is minimum. It is to be noted that, we have already seen from previous section $\beta = 25^\circ$ is a better configuration than $\beta = 20^\circ$ (i.e. single-cone). As β increases their is increase in shock strength, and hence values of drag and local heat transfer coefficient increases after formation shock at second cone angle (β). We can notice that, increase in the value of drag coefficient after formation of second shock is significant, which reduces accuracy of landing. Table 4 shows the average and peak values of heat flux over the entire capsule wall. Peak heat flux values are identical, whereas average heat flux is found to be minimum for the case of $\beta = 25^\circ$. Thus, we can conclude that bi-cone capsule with $\alpha = 20^\circ$ and $\beta = 25^\circ$ is an optimized configuration.

Optimizing Bluntness

We have shown that, bi-cone capsule with $\alpha = 20^\circ$ and $\beta = 25^\circ$ is an optimum configuration. Hence, we further carried out the optimization study based on the variation of bluntness of the bi-cone capsule keeping $\alpha = 20^\circ$ and $\beta = 25^\circ$. Figure 11 and 12 shows the variation of drag and heat transfer coefficient along the capsule wall for different bluntness values. Table 5 shows the average and peak heat flux over the entire capsule surface. It is found that peak and average heat flux value is lower for the case with blunt-

Average C_h	60km			70km		
Ma	**10**	**15**	**20**	**10**	**15**	**20**
Single-cone	0.014	0.012	0.011	0.037	0.036	0.036
Bi-cone	0.1	0.008	0.007	0.032	0.03	0.029
%Deviation	29.19	32.39	34.54	15.56	18.41	19.74

TABLE 3. AVERAGE HEAT TRANSFER COEFFICIENT C_H DATA AT 60 KM AND 70 KM ALTITUDE FOR VARIOUS FLOW CONDITIONS.HERE, ABSOLUTE VALUES ARE PRESENTED FOR SINGLE-CONE AND BI-CONE CONFIGURATIONS. DEVIATION DENOTES THE % OF DEVIATION OF BI-CONE WITH SINGLE-CONE CONFIGURATION RESULTS.

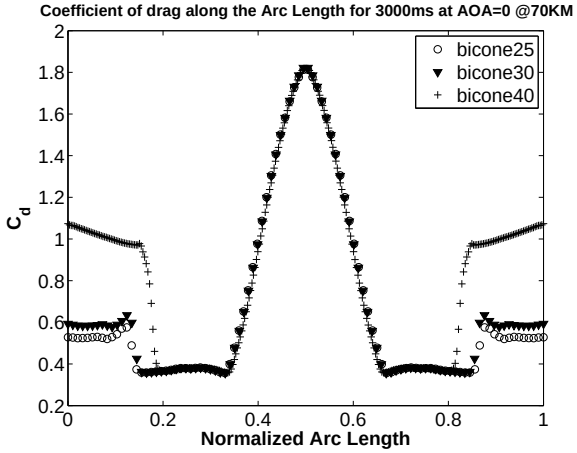

(a)

FIGURE 9. β VARIATION: DRAG COEFFICIENT ALONG CAPSULE WALL AT 70KM

	$\alpha = 20°$			
β:	20°	25°	30°	40°
Average Heat Flux (*KW/m2*)	37.53477578	31.69590268	31.99880201	33.10359396
Peak Heat Flux (*KW/m2*)	83.999	58.415	58.52	58.325

TABLE 4. AVERAGE AND PEAK HEAT FLUX VALUES AT 70KM AND MA = 10 FOR DIFFERENT β (KEEPING α CONSTANT).

ness = 0.5. Whereas considering drag, the case with 0.25 bluntness is found to be minimum from Fig. 11. Therefore, we investigate an another parameter, the average drag coefficient which is also found to have a lower value for the bluntness = 0.25.

Based on the application, one can choose an optimized geometry. For example, a re-entry mission requiring higher

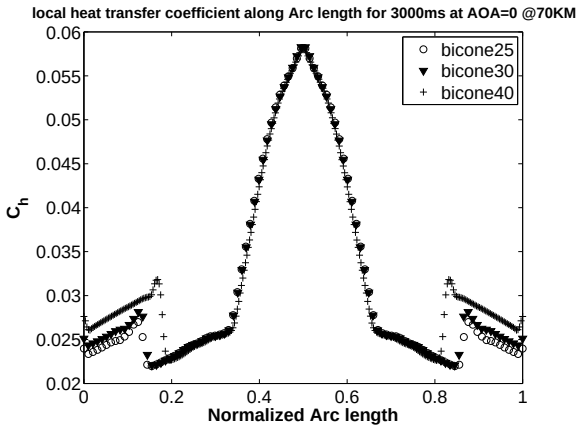

(a)

FIGURE 10. β VARIATION: LOCAL HEAT TRANSFER COEFFICIENT ALONG CAPSULE WALL AT 70KM.

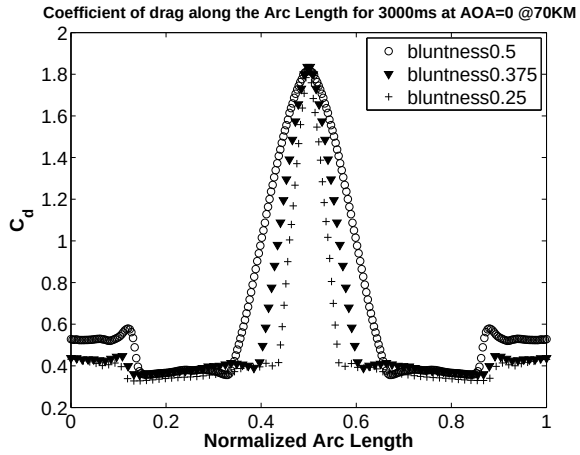

(a)

FIGURE 11. BLUNTNESS VARIATION: DRAG COEFFICIENT ALONG CAPSULE WALL AT 70KM.

accuracy, drag prediction plays an important role whereas for a mission requiring higher safety, heat load is more of concern. Thus, one can choose bluntness of 0.25 for the mission requiring the landing to be within a specified area (i.e. a more accurate landing) and the bluntness of 0.5 can be chosen for the cases where lower localized heating is desired which in turn helps to reduce the additional cost of thermal protection systems.

CONCLUSIONS

We have carried out the optimization of capsule geometry configuration based on the values of drag and heat trans-

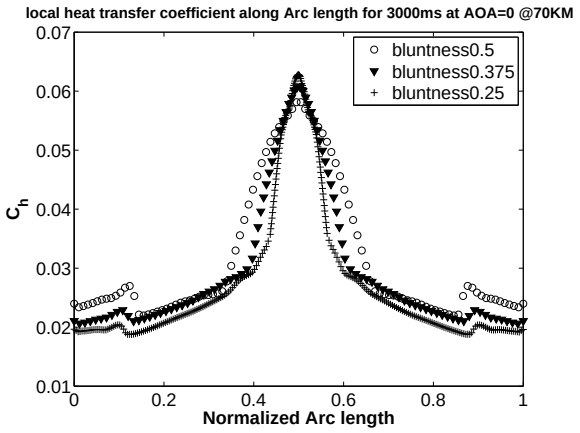

(a)

FIGURE 12. BLUNTNESS VARIATION: LOCAL HEAT TRANSFER COEFFICIENT ALONG CAPSULE WALL AT 70KM.

	$\alpha = 20^\circ$ and $\beta = 25^\circ$		
Bluntness:	0.25	0.375	0.5
Average Heat Flux (KW/m2)	32.88851678	32.31602013	31.69590268
Peak Heat Flux (KW/m2)	62.883	60.855	58.415
Average of Drag Coefficient	0.644	0.662	0.682

TABLE 5. AVERAGE AND PEAK HEAT FLUX AND AVERAGE DRAG COEFFICIENT VALUES AT 70KM AND MA $= 10$ FOR DIFFERENT BLUNTNESS (FOR $\alpha = 20^\circ$ AND $\beta = 25^\circ$).

fer coefficient. The results of single and bi-cone has shown a higher value of heat flux for the single cone configuration in comparison to the bi-cone. Further, we observed from the second-cone angle optimization study that the bi-cone with $\alpha = 20^\circ$ and $\beta = 25^\circ$ is an optimized configuration, when heat loads are of major concern. Lower bluntness gives a better accuracy whereas a higher value gives a lesser heat load on the re-entry vehicle.

Numerical Methods are found to be better tool for optimizing purpose in light of less experimental data available for high altitude flows. Inclusion of slip boundary conditions extends the continuum Navier-Stokes to slip-flow regime, hence it improves the numerical techniques required to handle rarefied flows.

Although the current test cases are in the early slip flow regime, the first-order non-equilibrium boundary conditions are not sufficient to accurately describe the non-equilibrium gas flow physics. We may need to incorporate both the higher-order boundary conditions as well as the non-linear constitutive relations into the Navier-Stokes equations framework to report better predictions for re-entry gas flows. In future, we hope to investigate for existing and new theoretical models based on the results of numerical simulation to generalize our optimization procedure.

ACKNOWLEDGMENT

The research leading to these results has received funding from the Department of Science and Technology (DST) India under the Fast Track Young Scientist-Engineering Science Scheme SERB/F/2684. The authors HRG and AA would like to acknowledge the assistance provided by the funding agency Department of Higher Education, Ministry of Human Resource Development, Government of India.

REFERENCES

[1] Launius, R. D., and Jenkins, D. R., 2012. *Coming Home: Reentry and Recovery from Space*. Government Printing Office.

[2] John, B., Mathew, D., Deependran, B., Joseph, G., Nair, C. R., and Ninan, K., 2011. "Medium-density ablative composites: processing, characterisation and thermal response under moderate atmospheric re-entry heating conditions". *Journal of Materials Science,* ***46***(15), pp. 5017–5028.

[3] Sippel, M., Schwanekamp, T., Trivailo, O., and Lentsch, A., 2013. "Progress of spaceliner rocket-powered high-speed concept". In 64th International Astronautical Congress.

[4] Schwanekamp, T., Meyer, F., Reimer, T., Petkov, I., Tröltzsch, A., and Siggel, M., 2014. "System studies on active thermal protection of a hypersonic suborbital passenger transport vehicle".

[5] Allen, H. J., and Eggers, A., 1958. *A study of the motion and aerodynamic heating of ballistic missiles entering the earth's atmosphere at high supersonic speeds*. NACA.

[6] Lin, T. C., Grabowsky, W. R., and Yelmgren, K. E., 1984. "The search for optimum configurations for re-entry vehicles". *Journal of Spacecraft and Rockets,* ***21***(2), pp. 142–149.

[7] Tang, W., Orlowski, M., Longo, J. M., and Giese, P., 2001. "Aerodynamic optimization of re-entry capsules". *Aerospace science and technology,* ***5***(1), pp. 15–25.

[8] Clauser, F., 1946. *Preliminary Design of an Experimental World-Circling Spaceship*. Douglas Aircraft Company Engineering Division.

[9] Ross, J. C., Heineck, J. T., Burnside, N., Sellers, M. E., Halcomb, N., Garbeff, T., Yamauchi, G., and Kushner, L. "Comprehensive Study of the Flow Around a Simplified Orion Capsule Model". In *31st AIAA Ap-*

plied Aerodynamics Conference. American Institute of Aeronautics and Astronautics. 00004.

[10] Hollis, B. R., Berger, K. T., Berry, S. A., Brauckmann, G. J., Buck, G. M., DiFulvio, M., Horvath, T. J., Liechty, D. S., Merski, N., Murphy, K. J., et al., 2014. "Entry, descent and landing aerothermodynamics: Nasa langley experimental capabilities and contributions".

[11] Votta, R., Schettino, A., Bonfiglioli, A., Levin, D. A., Wysong, I. J., and Garcia, A. L., 2011. "Advanced models for prediction of high altitude aero-thermal loads of a space re-entry vehicle". In AIP Conference Proceedings-American Institute of Physics, Vol. 1333, p. 1343.

[12] Votta, R., Schettino, A., Ranuzzi, G., and Borrelli, S. F., 2009. "Hypersonic low-density aerothermodynamics of orion-like exploration vehicle". *Journal of Spacecraft and Rockets,* ***46***(4), pp. 781–787.

[13] Weller, H. G., Tabor, G., Jasak, H., and Fureby, C., 1998. "A tensorial approach to computational continuum mechanics using object-oriented techniques". *Computers in physics,* ***12***(6), pp. 620–631.

[14] Jasak, H., 2010. "Openfoam: a year in review". In 5th OPENFOAM Workshop, Gothenburg, Sweden, June, pp. 21–24.

[15] Casartelli, E., and Mangani, L., 2013. "Object-oriented open-source cfd for turbomachinery applications: A review and recent advances". In ASME Turbo Expo 2013: Turbine Technical Conference and Exposition, American Society of Mechanical Engineers, pp. V06BT37A036–V06BT37A036.

[16] Kurganov, A., and Tadmor, E., 2000. "New high-resolution central schemes for nonlinear conservation laws and convection–diffusion equations". *Journal of Computational Physics,* ***160***(1), pp. 241–282.

[17] Kurganov, A., Noelle, S., and Petrova, G., 2001. "Semidiscrete central-upwind schemes for hyperbolic conservation laws and hamilton–jacobi equations". *SIAM Journal on Scientific Computing,* ***23***(3), pp. 707–740.

[18] Greenshields, C. J., Weller, H. G., Gasparini, L., and Reese, J. M., 2010. "Implementation of semi-discrete, non-staggered central schemes in a colocated, polyhedral, finite volume framework, for high-speed viscous flows". *International journal for numerical methods in fluids,* ***63***(1), pp. 1–21.

[19] Bansal, A., Feldick, A., and Modest, M., 2012. "Simulation of hypersonic flow and radiation over a mars reentry vehicle using openfoam". In 50th AIAA Aerospace Sciences Meeting including the New Horizons Forum and Aerospace Exposition: ISBN, pp. 978–1.

[20] Nakao, S., Kashitani, M., Miyaguni, T., and Yamaguchi, Y., 2014. "A study on high subsonic airfoil flows in relatively high reynolds number by using openfoam". *Journal of Thermal Science,* ***23***(2), pp. 133–137.

[21] SPALART, P., and ALLMARAS, S., 1992. "A one-equation turbulence model for aerodynamic flows". In *30th Aerospace Sciences Meeting and Exhibit*, Aerospace Sciences Meetings. American Institute of Aeronautics and Astronautics, Jan. 05351.

[22] Nikaido, B. E., Murman, S. M., and Garcia, J., 2015. "OpenFOAM Simulations of Atmospheric-Entry Capsules in the Subsonic Regime". In *53rd AIAA Aerospace Sciences Meeting*, AIAA SciTech. American Institute of Aeronautics and Astronautics, Jan. 00000.

[23] Maxwell, J. C., 1878. "On stresses in rarefied gases arising from inequalities of temperature.". *Proceedings of the Royal Society of London,* ***27***(185-189), pp. 304–308.

[24] Le, N. T., White, C., Reese, J. M., and Myong, R. S., 2012. "Langmuir–maxwell and langmuir–smoluchowski boundary conditions for thermal gas flow simulations in hypersonic aerodynamics". *International Journal of Heat and Mass Transfer,* ***55***(19), pp. 5032–5043.

[25] Mahdavi, A.-M., Le, N. T., Roohi, E., and White, C., 2014. "Thermal rarefied gas flow investigations through micro-/nano-backward-facing step: Comparison of dsmc and cfd subject to hybrid slip and jump boundary conditions". *Numerical Heat Transfer, Part A: Applications,* ***66***(7), pp. 733–755.

[26] Le, N., Greenshields, C. J., and Reese, J., 2012. "Evaluation of nonequilibrium boundary conditions for hypersonic rarefied gas flows". In Progress in Flight Physics, Vol. 3, EDP Sciences, pp. 217–230.

[27] Kalimuthu, R., 2003. Surface pressure measurement results on the sre (biconic) configuration at mach= 5. vikram sarabhai space center. Tech. rep., Internal Rept. VSSC/ATFD/TM_SRE/078/2003, Thiruvananthpuram, India.